JBC Papers in Press. Published on June 29, 2016 as Manuscript M116.733337
The latest version is at http://www.jbc.org/cgi/doi/10.1074/jbc.M116.733337

Heme-Independent Redox Sensing by the Heme-Nitric Oxide/Oxygen Binding Protein (H-NOX) from *Vibrio cholerae**

Roma Mukhopadyay[‡], Nilusha Sudasinghe[§], Tanner Schaub[§], and Erik T. Yukl[‡,1]

[‡]Department of Chemistry and Biochemistry, New Mexico State University, Las Cruces, NM 88003.
[§]Chemical Analysis and Instrumentation Laboratory, New Mexico State University, Las Cruces, NM 88003

*Running title: *H-NOX Redox Sensing*

To whom correspondence should be addressed: Erik T. Yukl, Department of Chemistry and Biochemistry, 1175 N. Horseshoe Dr., Las Cruces, NM; Tel. 575 646-3176; Fax. 575 646-2649; E-mail: etyukl@nmsu.edu

Keywords: Heme, H-NOX, redox sensing

ABSTRACT

Heme nitric oxide/oxygen (H-NOX) binding proteins act as nitric oxide (NO) sensors among various bacterial species. In several cases, they act to mediate communal behavior such as biofilm formation, quorum sensing and motility by influencing the activity of downstream signaling proteins such as histidine kinases (HisKa) in a NO-dependent manner. A H-NOX / HisKa regulatory circuit was recently identified in *Vibrio cholerae* and the H-NOX protein has been spectroscopically characterized. However, the influence of the H-NOX protein on HisKa autophosphorylation has not been evaluated. This process may be important for persistence and pathogenicity in this organism. Here we have expressed and purified the *V. cholerae* HisKa (HnoK) and H-NOX in its heme-bound (holo) and heme-free (apo) forms. Autophosphorylation assays of HnoK in the presence of H-NOX show that the holo protein in the Fe(II)-NO and Fe(III) forms is a potent inhibitor of HnoK. Activity of the Fe(III) form and aerobic instability of the Fe(II) form suggested that *Vc* H-NOX may act as a sensor of redox state as well as NO. Remarkably, the apo protein also showed robust HnoK inhibition that was dependent on the oxidation of cysteine residues to form disulfide bonds at a highly conserved zinc site. The importance of cysteine in this process was confirmed by mutagenesis, which also showed that holo Fe(III), but not Fe(II)-NO, H-NOX relied heavily upon cysteine for activation. These results highlight a heme-independent mechanism for activation of *Vc* H-NOX that implicates this protein as a dual redox / NO sensor.

The toxic gas nitric oxide (NO)[2] is now known to play multiple roles in human physiology (1). Toward the end of the 20[th] century, it was identified as the cardiovascular signaling agent originally referred to as "endothelium-derived relaxing factor" (2), which mediates vasodilation via interaction with the heme domain of soluble guanylate cyclase (sGC) (3). Binding of NO to the Fe(II) heme iron results in cleavage of the proximal Fe-His bond, yielding a 5-coordinate Fe(II)-NO species and stimulating activity of the catalytic domain to produce the secondary messenger cyclic GMP (cGMP) (4). Depending on the species and lifestyle, bacteria may also encounter NO as the product of a host immune response or as an intermediate of denitrification. Therefore, it is not surprising that many bacterial species have evolved mechanisms for sensing NO and initiating physiological responses to evade or detoxify it.

The heme-nitric oxide/oxygen binding (H-NOX) proteins are bacterial homologues to the heme domain of mammalian sGC. Since their identification by a bioinformatics search in 2003 (5), the H-NOX proteins have been the subject of intense study resulting in significant insight into their function and structure. Generally, the NO-sensing H-NOXs have been found to govern communal behaviors such as biofilm formation,

quorum sensing, motility and symbiosis in response to NO (6-10). This occurs by modulation of downstream signaling proteins such as histidine kinases, diguanylate cyclases or phosphodiesterases. The former is involved in initiating phosphorylation signaling cascades while the latter two enzymes control the levels of the secondary messenger cyclic-di-GMP (c-di-GMP).

Perhaps the best studied H-NOX signaling system comes from *Shewanella oneidensis* where genes encoding the H-NOX and histidine kinase (*So* HnoK) are adjacent to one another. Elegant phosphotransfer profiling experiments elucidated the signaling pathway beginning with HnoK autophosphorylation (9). *So* HnoK phosphorylates the c-di-GMP phosphodiesterase HnoB, activating it to hydrolyze c-di-GMP and inhibit biofilm formation. HnoD, an inhibitor of HnoB, is also phosphorylated by HnoK, relieving its inhibitory activity. H-NOX in the Fe(II)-NO state strongly inhibits HnoK autophosphorylation (11), resulting in an increase in c-di-GMP levels and biofilm formation in response to NO. As for sGC, rupture of the Fe-His bond upon NO binding is predicted to activate H-NOX for inhibition of HnoK. Indeed, crystal structures of *So* H-NOX in the Fe(II) and Fe(II)-NO states identified structural rearrangements accompanying NO binding and proximal His displacement (12).

In *Vibrio cholerae*, the genes encoding this signaling pathway are conserved and phosphotransfer between *Vc* HnoK and *Vc* HnoB/D has been demonstrated *in vitro* (12). As a pathogen, resistance to host-derived NO would be a major adaptive advantage, making H-NOX signaling in this organism of potential therapeutic interest. However, the role of NO and *Vc* H-NOX in this signaling pathway have yet to be evaluated. Further, despite significant sequence homology (33% identity), Fe(II) *Vc* H-NOX is reactive with O_2 (13), auto-oxidizing in air whereas *So* H-NOX in the Fe(II) state is unreactive toward O_2 (11). This property suggests a possible role for *Vc* H-NOX as a redox sensor, a function that has been proposed for *Nostoc puntiforme* H-NOX for the same reason (14). Here we set out to evaluate the function of H-NOX as a NO and/or redox sensor by investigating its inhibitory activity toward HnoK autophosphorylation. We also assess the activity of a heme-free preparation (apo H-NOX) under reducing and oxidizing conditions. The results identify both heme-dependent and heme-independent mechanisms of inhibition, the latter relying on the reversible oxidation of Cys residues near a conserved Zn binding site.

RESULTS

Expression, Purification and Characterization of V. Cholerae H-NOX and HnoK — Both H-NOX and HnoK were over-expressed with a His-tag at the N-terminus and purified by Ni-affinity chromatography to yield reasonably pure preparations (Fig. 1A). Purification of holo-H-NOX required the addition of hemin to the culture medium whereas apo-protein was isolated from cultures grown in LB medium without supplementation (Fig. 1B). The apo protein was highly stable and soluble, with identical secondary structure to the holo protein as determined by circular dichroism (Fig. 1C). The UV-vis spectrum of holo H-NOX as-isolated has a Soret maximum at 412 nm, consistent with a predominantly Fe(III) heme. The Fe (II)-NO form was generated by anaerobic reduction with ascorbate in the presence of the NO donor DEA-NONOate. After desalting, the absorbance spectrum exhibited a Soret maximum at 398 nm that was stable in air for many hours. This is consistent with a 5-coordinate Fe(II)-NO complex with spectral characteristics essentially identical to those previously described (13) (Fig. 1B). Finally, HnoK autokinase activity was assessed in the presence and absence of 1 mM DTT (Fig. 1D). The results show robust autophosphorylation over time that is very slightly enhanced (<10%) in the presence of DTT.

H-NOX from *V. cholerae* is known to bind a structural zinc ion, presumably coordinated to C149, C174 and C182. These residues are conserved in the structure of *S. oneidensis* H-NOX (12), which was used to construct a homology model of this site in *Vc* H-NOX (Fig. 2). Metal content analysis by ICP-OES (Fig. 3) demonstrates that holo WT H-NOX binds approximately stoichiometric zinc and iron, consistent with complete heme and zinc incorporation. Apo H-NOX also binds stoichiometric zinc. However, the iron content of the apo protein was comparable to that of the buffer blank, consistent with the extremely weak Soret absorbance (Fig 1B) suggesting less than

0.03 equivalents of heme is bound to the apo protein.

Inhibition of HnoK autophosphorylation by WT H-NOX — To test whether Vc H-NOX acts to inhibit HnoK signaling, HnoK autophosphorylation was measured in the presence of varying concentrations of WT holo H-NOX in the Fe(III) and Fe(II)-NO forms (Fig. 4A). The results show that both are potent inhibitors of HnoK autophosphorylation, consistent with similar measurements for *S. oneidensis* homologues (11). Surprisingly, apo H-NOX also weakly inhibited HnoK autokinase activity (Fig. 4A). The limited fraction of holo protein present in apo preparations (< 3%) likely contributes to this but is unable to account for the degree of inhibition observed, indicating the presence of both heme-dependent and heme-independent mechanisms of HnoK inhibition by H-NOX. The Fe(II) form of *Vc* H-NOX auto-oxidizes relatively rapidly in the presence of oxygen (13), precluding its analysis by this assay. In fact, the presence of excess reductant in the form of 1 mM DTT results in the degradation of the heme upon exposure to air as shown by the decay of absorbance features over time (Fig. 5A). Similar results were observed using ascorbate and reduced glutathione.

Taken together, the above data suggested a potential role for apo H-NOX as a redox sensor, most likely through the reversible oxidation of cysteine residues. To test this, we compared the inhibitory activity of reduced and oxidized apo H-NOX. The reduced form was prepared by incubation with excess DTT followed by desalting to remove excess reductant. The DTT-reduced and desalted protein was then incubated with HOCl, H_2O_2 or diamide and desalted a second time to generate the oxidized forms. Remarkably, DTT reduction completely eliminated the inhibitory activity of apo H-NOX while oxidation restored it to varying degrees depending on the oxidant used (Fig. 4B). HOCl treatment resulted in a form of apo H-NOX with activity comparable to that of the holo forms. Diamide was also an effective activator while H_2O_2 treatment resulted in only modest inhibitory activity. Importantly, oxidative activation of apo H-NOX was completely reversible in all cases by including 1 mM DTT in autophosphorylation reactions at the highest concentration of oxidized apo H-NOX.

Inhibition of HnoK autophosphorylation by C177A H-NOX — In addition to the three conserved cysteine residues that likely coordinate the zinc ion (C149, C174 and C182) (12), *Vc* H-NOX has a fourth cysteine (C177) that is not strictly conserved. Homology modeling suggests that this residue is very near the zinc site and is surface exposed (Fig 2). To assess their importance to redox sensing by *Vc* H-NOX, these cysteine residues were systematically mutated. Mutants of C149 and C182 were completely insoluble and could not be purified. C174S was somewhat soluble and stable in the reduced state but precipitated immediately upon addition of oxidant. These results suggest that an intact Cys-ligated zinc site is important for protein folding. However, mutation of the non-conserved C177 to alanine was well tolerated with no apparent change in zinc incorporation (Fig. 3B), heme ligation (Fig 6A), heme reactivity (Fig. 6B) or overall structure (Fig. 1C).

Holo and apo C177A were assayed for their ability to inhibit HnoK under the same conditions used for the WT (Fig 4C and D). Whereas the activity of holo C177A Fe(II)-NO was not significantly affected by the mutation, the Fe(III) form showed considerably weaker activity than WT. For the apo protein, HOCl treatment was still sufficient to activate C177A H-NOX to near-WT levels while diamide and H_2O_2 had no significant effect. The results indicate that C177 is important for H-NOX activity in both the holo Fe(III) and apo states. However, it is not absolutely required since NO binding to the holo or HOCl treatment of the apo is still capable of activating the mutant to near-WT levels.

Reduced Thiol and Zn Content — In order to determine a role for H-NOX Cys residues in Zn coordination and reversible oxidative activation, WT and C177A holo and apo H-NOX in various forms were compared in terms of thiol and zinc content (Fig. 3). DTNB was used to quantify the amount of reactive thiol under both native and denaturing conditions, allowing observation of solvent accessible and total thiol content, respectively. Comparison of reduced WT and C177A H-NOX samples demonstrate that C177 is primarily responsible for DTNB reactivity under native conditions. The other Cys residues are likely unreactive due to zinc coordination (Fig. 2). The native DTNB signal in WT is essentially lost

after treatment with any of the oxidants studied, indicating that C177 is particularly sensitive to oxidation.

The degree of total Cys oxidation varied with sample type. Both WT and C177A apo proteins were predominantly reduced as-isolated, consistent with the weak inhibitory activity of this form (Fig. 4A). Conversely, the holo WT protein in Fe(III) and Fe(II)-NO forms was highly oxidized, with only ~ 1 equivalent of reactive thiol while C177A holo proteins were predominantly reduced. This highlights the general trend that C177A H-NOX is more resistant to oxidation than the WT. The similar levels of reduced thiol in Fe(III) and Fe(II)-NO forms for both proteins argues against the significant formation of S-NO or other oxidized products in response to NO. Only HOCl treatment resulted in virtually complete oxidation of both proteins. Remarkably, no significant zinc loss was observed for any of the oxidized forms, despite the complete oxidation of putative zinc ligands in the HOCl-treated proteins. These experiments were repeated with a tag-free preparation of H-NOX to discount the possibility of Zn coordination by the His-tag. Here again, while DTNB assay showed 4.0 and 0.7 equivalents of total reduced thiol for reduced and oxidized proteins, respectively, both were found to coordinate 1.0 equivalent of Zn.

Mass Spectrometry — The oxidized and reduced forms of WT and C177A apo H-NOX were further characterized by mass spectrometry (Fig. 7). The isotopic signal cluster for isolated +22 charge state was calculated using MS-Isotope (Baker, P.R. and Clauser, K.R. http://prospector.ucsf.edu) and superimposed over the collected mass spectrum to give an estimate of monoisotopic mass. The spectrum of the WT reduced protein was consistent with its calculated mass of 22,820.49 (average observed mass measurement error of 2.5 ppm). Oxidation by H_2O_2 and diamide resulted in negative shifts of the observed mass spectral signals, that correspond to the loss of two and three protons, respectively. Those observations suggest formation of a single intramolecular disulfide bond for H_2O_2-treated protein and a mixture of singly and doubly disulfide bonded protein after diamide treatment. Surprisingly, diamide treatment also resulted in formation of a +32 Da adduct in the WT protein that was not observed for C177A (Fig. 8). The nature of this modification is still under investigation, but likely represents an oxidized adduct of C177. The same adduct is observed if the non-sulfur reductant TCEP is used, ruling out addition of a sulfur atom from residual DTT (Fig. 8C). HOCl treatment of the WT protein resulted in the largest shift, consistent with the loss of four protons and the complete formation of 2 intramolecular disulfide bonds. As such, FT-ICR MS observations are consistent with DTNB and autophosphorylation assays demonstrating a close correlation between the degree of Cys oxidation and the inhibitory activity of apo H-NOX. With the exception of the diamide-oxidized sample, no evidence of other oxidative modifications such as Cys sulfonation or Met sulfoxide were observed. This is consistent with the primary mode of oxidative modification being the formation of disulfide bonds.

The spectrum of reduced C177A H-NOX is consistent with its calculated monoisotopic mass of 22,788.52. Upon oxidation with H_2O_2 or diamide, there is very little change in this spectrum, indicative of the loss of no more than one proton, and consistent with DTNB and activity assays indicating that these oxidants have no significant effect on the mutant protein. However, treatment of C177A H-NOX with HOCl resulted in a significant shift consistent with the loss of three protons relative to the reduced mass. Further, we observe additional signals consistent with the formation of a disulfide-linked dimer. This observation was confirmed by non-reducing SDS-PAGE, which showed a significant amount of a dimeric species for the HOCl-oxidized C177A H-NOX that was not observed in other samples (Fig. 9). These results indicate the formation of one intramolecular and one intermolecular disulfide bond in HOCl-treated C177A H-NOX.

Protein-protein Interactions between Apo H-NOX and HnoK — The loss of inhibitory activity of apo H-NOX upon reduction could be due to disruption of HnoK binding. Alternatively, binding may be unaffected, with apo H-NOX assuming a non-inhibitory conformation upon Cys reduction. In order to differentiate between these two scenarios, pull-down assays were performed. Untagged apo H-NOX in the reduced and HOCl-oxidized states was incubated with His-tagged HnoK followed by binding to Ni-NTA, washing and elution (Fig. 10). The results show increased

recovery of H-NOX in the HOCl-oxidized relative to the reduced form, indicating a more stable interaction with HnoK. Therefore, it appears that reduction of apo H-NOX weakens its ability to bind HnoK, resulting in a loss of inhibition.

DISCUSSION

Here we have assayed the ability of H-NOX from *Vibrio cholerae* to inhibit autophosphorylation of the signaling kinase HnoK. The results demonstrate that both the holo Fe(III) and Fe(II)-NO WT forms are equally good inhibitors, similar to what has been observed in *Shewanella oneidensis* (11). The sensitivity of holo Fe(II) H-NOX to oxygen suggested that *Vc* H-NOX may act as a redox sensor while the observed heme degradation suggested that the apo form may be relevant to H-NOX redox signaling. Indeed, apo H-NOX could be reversibly activated by Cys oxidation, and the extent of oxidation as determined by DTNB assay correlated well with inhibitory activity. HOCl was a particularly effective oxidant, leading to inhibition of HnoK to a level comparable to that of the holo proteins. Mass spectrometry was further used to identify the formation of intramolecular disulfide bonds as the primary mode of Cys oxidation, which appears to be necessary and sufficient for apo H-NOX binding and inhibition of HnoK. To our knowledge, this is the first description of a heme-independent sensing function for a H-NOX protein, implicating it as a dual NO and redox sensor.

The reversible oxidation of Cys residues has emerged as a relatively widespread mechanism of redox sensing (15). Cys-coordinated Zn sites like that in H-NOX are particularly good redox sensors as Zn coordination stabilizes the reactive thiolate (16,17) and places Cys residues in close proximity for disulfide formation. Oxidation of cysteine ligands to zinc can activate or inhibit a wide variety of protein functions through various oxidative modifications that may or may not result in zinc loss (15,18). Both HOCl and H_2O_2 are highly reactive toward cysteine thiols and have been shown to activate the redox-regulated chaperone Hsp33 by inducing the formation of disulfide bonds, likely through a Cys sulfenic acid intermediate (19-21). Diamide is a relatively thiol-specific reagent that induces disulfide bond formation or S-thiolation (22) via exchange reactions not unlike those catalyzed by glutathione (23). All three oxidants were found to activate apo H-NOX to varying degrees.

The well-characterized oxidative activation of Hsp33 is similar to what we observe in apo *Vc* H-NOX. The chaperone activity of Hsp33 is activated upon oxidation of four conserved zinc-coordinating cysteine residues to form two intramolecular disulfide bonds, leading to zinc dissociation and protein dimerization (19,24-26). While H_2O_2 treatment results in partial cysteine oxidation and Zn loss, it is insufficient to activate Hsp33. Full activation requires unfolding conditions such as heat or denaturants in addition to H_2O_2 in order to fully oxidize all four cysteines and promote dimerization that leads to an active chaperone (20). Alternatively, HOCl treatment alone is sufficient to fully oxidize and activate Hsp33 (21), presumably due to the exceedingly rapid reaction of HOCl with thiol groups (27), allowing for the oxidation of only transiently exposed residues. The most striking difference between the oxidative activation of apo H-NOX versus Hsp33 is the observation that zinc is never lost from the H-NOX protein, despite the complete oxidation of cysteine ligands. An investigation of the modeled zinc site in *Vc* H-NOX reveals the presence of several potential zinc ligands nearby, including conserved histidine and glutamate residues (Fig. 2). We hypothesize that these residues can substitute for the cysteine ligands upon oxidation, posing the intriguing possibility of a ligand switch during oxidation that may mediate local structural rearrangement. However, a definitive assignment of zinc coordination in reduced and oxidized states awaits high-resolution structural data or analysis by extended X-ray fine structure (EXAFS).

Based on the data presented, we suggest a model of apo H-NOX activation involving the successive oxidation of cysteine residues to form intramolecular disulfide bonds (Fig. 11). A precise description of connectivity among cysteine residues will require careful labeling and LC/MS/MS analysis, experiments that are underway in our laboratories. However, some inferences about the nature of disulfide bonding in activated apo H-NOX may be made based on the current data.

Treatment of WT apo H-NOX with H_2O_2 or diamide results in partial activation, the loss of

two DTNB-reactive thiols and two or three protons, respectively. As no significant dimerization is observed, we conclude that these observations are due to the formation of a single intramolecular disulfide bond. The observation that these reagents have no effect on C177A apo H-NOX indicates that C177 is involved in this bond. Based on the homology structure of Vc H-NOX (Fig. 2), C174 is positioned very near to C177 and is the most likely candidate for a disulfide bond partner. On the other hand, treatment with HOCl leads to complete activation of WT and C177A apo H-NOX, oxidizes virtually all DTNB-reactive thiol and results in the loss of three and four protons for mutant and WT proteins, respectively. In the WT, we attribute this to the formation of 2 intramolecular disulfide bonds, as we observe no significant dimerization by mass spectrometery or non-reducing SDS-PAGE. Based on the previous discussion, this second disulfide would be between C149 and C182 and is required for complete activation. If true, this disulfide is also present in HOCl-treated C177A H-NOX. However, in this case C174 forms an intermolecular disulfide as it can no longer form an intramolecular disulfide with residue 177. Remarkably, this species appears to be an active inhibitor of HnoK autophosphorylation, highlighting the major role of the C149-C182 disulfide bond in the activation process.

The function of H-NOX proteins as NO sensors modulating biofilm formation has been convincingly demonstrated *in vivo* for *Legionella pneumophila* (6), *Shewanella woodyi* (8), *Vibrio harveyi* (7), and *Shewanella oneidensis* (9). To our knowledge, there is no *in vivo* characterization of H-NOX signaling in *V. cholerae*, and the role of H-NOX in redox sensing has not been evaluated for any of the above organisms. However, the Fe(III) form is an equally good inhibitor of histidine kinase autophosphorylation as the Fe(II)-NO form for both *V. cholerae* and *S. oneidensis* (11) systems, consistent with a redox sensing function. This observation is contrary to the model of H-NOX activation that requires rupture of the proximal Fe-His bond upon NO binding. Our results showing the dramatically decreased inhibitory activity of the Fe(III) form of C177A H-NOX relative to WT helps to reconcile this observation. The Cys residues of WT Fe(III) H-NOX are almost completely oxidized while those of Fe(III) C177A H-NOX were fully reduced. Therefore, much of the activity of the Fe(III) form may be mediated by a heme-independent mechanism involving cysteine oxidation. Although C177 is not conserved in *S. oneidensis*, there is a fourth cysteine residue near the zinc binding site at position 141 that could fill the same role as C177 in *V. cholerae* H-NOX. In this regard, it will be of interest to evaluate whether heme-independent activation mechanisms are present in other H-NOX homologues.

In conclusion, we have shown that apo H-NOX from *Vibrio cholerae* can act as a redox sensor *in vitro* through the formation of disulfide bonds upon exposure to oxidants. Exposure to oxidative stress is likely to occur in both the marine (28) and human host (29,30) environments that this organism inhabits. Whether oxidant levels in these environments would be sufficient to activate H-NOX by the proposed mechanism remains uncertain. However, it is worth noting that the production of exopolysaccharides during biofilm formation has been shown to confer resistance to HOCl stress in *V. cholerae* (31). Thus, redox sensing would seem a logical function for H-NOX. The physiological role of cysteine-based redox sensing by H-NOX proteins in *V. cholerae* will have to be evaluated by genetic manipulation. However, it is clear that the formation of disulfide bonds in apo H-NOX leads to an active inhibitor of HnoK, making this process mechanistically relevant. Further, activity in apo H-NOX provides the opportunity to structurally characterize an active form of the protein by nuclear magnetic resonance (NMR). This is particularly important for the H-NOX family, since these proteins have proven very difficult to crystallize. Structural characterization will provide additional insight into this unexpected function in *V. cholerae* H-NOX.

EXPERIMENTAL PROCEDURES

Expression and Purification of Proteins — The full-length WT *Vc* H-NOX gene was amplified by PCR from genomic DNA using the following primers: 5'-ACTATGGTACCATGAAAACAAGCGCAAGT-3' Fwd and 5'-GCTATGGATCCTCATGATGGCAAAAATTC-3' Rev. The PCR product was cloned into a pET-

45(b)+ vector (Novagen) using *Acc651* and *BamH1* restriction sites to yield a N-terminal 6 His-tagged constructed and transformed into BL21 *E coli* cells. The cells were grown in LB medium at 37°C to an OD of 0.4 and induced with 400 µM IPTG. For holo protein expression, 30 mg of hemin dissolved in 3 ml of 10 mM NaOH was added at this time. After induction, cells were grown at 18° C overnight. Cells were pelleted by centrifugation at 4200 rpm for 20 min at 4° C, resuspended in lysis buffer (50 mM sodium phosphate pH 7.5, 300 mM NaCl, 10 mM imidazole, 5% glycerol) and lysed by sonication on ice. Cell debris was removed by centrifugation at 25,000 x g for 20 min. Cleared lysate was applied to a Ni-NTA column (ThermoScientific), washed with 10 column volumes (cv) of 50 mM sodium phosphate pH 8.0, 300 mM NaCl, 20 mM imidazole and eluted with a gradient of 20 – 250 mM imidazole. The protein was finally dialyzed into storage buffer (50 mM HEPES pH 8.0, 300 mM NaCl, 5% glycerol). Variants were generated using the Q5® site-directed mutagenesis kit (New England Biolabs, Inc.) and confirmed by DNA sequencing at the New Mexico State University sequencing facility. Holo and apo variants were expressed and purified using the same protocols as for the WT.

A construct for the expression of untagged *Vc* H-NOX was generated by amplifying the intact gene by PCR using the following primers: 5'-ACTATCATATGAAAACAAGCGCAAGTGA-3' Fwd and 5'-ACTATGGTACCTCATGATGGCAAAAATTC-3' Rev. The PCR product was cloned into a pCDFDuet™ vector (Novagen) using *NdeI* and *Acc65I* restriction sites. Expression in BL21 cells was identical to that of the tagged protein. Cells were resuspended in 50 mM tris pH 8.0, 150 mM NaCl, lysed and cell debris removed as above. Polyethyleneimine (PEI) was added to 0.5% to precipitate nucleic acid, which was removed by centrifugation at 25,000 x g for 20 min. Ammonium sulfate was added to 60% saturation and centrifuged as above. Ammonium sulfate pellets were resolubilized in 20 mM tris pH 8.0, centrifuged again to remove particulates and applied to a HiTrap Q HP column (GE Healthcare) and eluted on a gradient of NaCl. Fractions containing H-NOX were pooled and further purified by size exclusion chromatography on a HiPrep Sephacryl S-200 HR column (GE Healthcare) equilibrated with storage buffer.

The full-length *Vc* HnoK gene was amplified by PCR from genomic DNA using the following primers: 5'-ACTATGGTACCATGAGTGCCGAAGCGCAA-3' Fwd and 5'-ACTATCTGCAGTCAGATCGCAGGGAACAG-3' Rev. The PCR product was cloned into a pET-45(b)+ vector (Novagen) using *Acc651* and *Pst1* restriction sites to yield a N-terminal 6 His-tagged construct and transformed into BL21 *E coli* cells. Expression and purification procedures were identical to those for his-tagged apo H-NOX except for the inclusion of 1mM β-mercaptoethanol in the lysis buffer. HnoK was then further purified through a HiPrep Sephacryl S-200 HR size exclusion column (GE Healthcare) equilibrated with storage buffer plus 1 mM DTT.

Protein purity was assessed by SDS-PAGE and the concentrations of apo H-NOX and HnoK were determined using extinction coefficients at 280 nm of 24,485 and 25,310 M^{-1} cm^{-1}, respectively, calculated as previously described (32). An extinction coefficient of 107,770 $M^{-1}cm^{-1}$ at 412 nm was determined for the as-isolated holo Fe(III) form using the pyridine hemochrome assay (33). This value was then used to determine an extinction coefficient for the Fe(II)-NO form of 99,655 $M^{-1}cm^{-1}$. These values were used to determine the concentration of holo H-NOX.

Absorbance Spectroscopy — All spectra were collected on a Cary 60 UV-Vis spectrophotometer (Agilent). The Fe(II)-NO form was generated by anaerobic addition of ascorbic acid to 25 mM and diethylamine NONOate (DEA-NONOate) (Cayman Chemicals) to 2.0 mM and allowed to incubate for 1 hour in a septum-sealed tube. The sample was then desalted in an anaerobic glove bag using Zeba™ spin desalting columns (Pierce). In order to measure the response of H-NOX to DTT and air, 1 mM DTT was anaerobically added to 5 µM holo H-NOX in the Fe(III) form in an anaerobic glove bag. This was then sealed into an anaerobic cuvette to measure reduction and subsequently exposed to air to measure reaction with oxygen.

H-NOX Sample Preparation — Holo Fe(III) H-NOX was used as-isolated while Fe(II)-NO H-NOX was generated by anaerobic incubation with ascorbic acid and NONOate as described above.

Apo H-NOX in the DTT-reduced state was generated by incubation of 250 μM protein with 5 mM DTT for 30 min at room temperature followed by desalting into HEPES storage buffer. The oxidized forms were generated by diluting the reduced form as generated above to 150 μM and incubating with 1.5 mM hydrogen peroxide, sodium hypochlorite or diamide for 1 hr at room temperature followed again by desalting. The concentrations of hydrogen peroxide and sodium hypochlorite were determined from extinction coefficients ε_{240} = 43.6 $M^{-1}cm^{-1}$ (34) and ε_{292} = 350 $M^{-1}cm^{-1}$ (35), respectively. Protein concentrations were measured after the final desalting steps using the extinction coefficients listed above.

Metal Content Analysis — The holo and apo H-NOX proteins in various forms were diluted to 25 μM in 4M HNO_3 for overnight digestion at 70° C. Prior to metal analysis, samples were diluted 15-fold with deionized water. Samples were analyzed on a Perkin-Elmer 2100 DV inductively coupled plasma -optical emission spectrometer (ICP-OES), calibrated with a multi-element standard. The wavelengths for measuring Fe and Zn were 238.204 and 213.857 nm, respectively, and samples were measured in triplicate.

Circular Dichroism — Circular dichroism (CD) spectra were recorded at 20 °C using a Jasco-810 spectropolarimeter with a cuvette chamber regulated by a PTC-4235 Peltier device (Jasco). Each of the holo and apo WT and C177A mutants were diluted to 5 μM in 1 mM K_2HPO_4, pH 8.0, 30 mM NaCl in a 1-mm quartz cuvette. Spectra were acquired from 190 to 260 nm at 1 nm bandwidth, 2 sec response time, 0.5-nm data pitch, and 10 nm/min scan speed.

Assays for Cysteine Thiol — H-NOX DTT-reduced and oxidized by each of the oxidants above was diluted to 20 μM in 100 mM K_2HPO_4 pH 7.0, 1.0 mM EDTA and a final concentration of 0.08 mg/ml 5,5'-dithio-bis-[2-nitrobenzoic acid] (DTNB) and incubated for 15 min at room temperature. Denaturing conditions included 6 M guanidine hydrochloride in the assay buffer. Absorbance was measured at 410 - 420 nm and the amount of free sulfydryl groups was determined using ε_{412} = 14150 $M^{-1}cm^{-1}$ (36,37). Due to interference from heme cofactor absorbance, concentrations of free thiol in holo samples were measured by subtracting the spectrum of the holo protein acquired before DTNB addition from that acquired afterward.

Autophosphorylation Assays — The kinase activity of HnoK was assayed by the addition of 2 μCi ATP [γ-32P], 1 mM ATP and 5 mM $MgCl_2$ to 10 μM HnoK in HEPES storage buffer with or without 1 mM DTT at room temperature. Aliquots were quenched at time points 5, 15, 30, 45 and 60 min with 4X Laemmli sample loading buffer. SDS_PAGE was performed using 4-15% tris-glycine gels (Bio-Rad) run at 200 mV for 38 min. Gels were dried for an hour on a slab gel dryer. The dried gels were exposed overnight (16–24 h) on a Kodak phosphorimaging plate and imaged using a Storm Phosphorimager (Amersham) at 100 μm resolution and quantified using GelQuant.NET software provided by biochemlabsolutions.com. For H-NOX inhibition assays, final concentrations of the various H-NOX forms at 0, 10, 25, 50 and 75 μM were included in the HnoK assay mixtures and incubated for 1 hr prior to quenching and SDS-PAGE.

SDS-PAGE — The holo and apo H-NOX proteins as-isolated, as well as apo H-NOX in the reduced and oxidized forms were generated as above and diluted to 10 μM in 10 μl of HEPES storage buffer. Then 4 μl of gel loading dye containing DTT was added and samples loaded on 4-15% bis-tris SDS-PAGE gels (Life Technologies). DTT was omitted for non-reducing gels and 10 μM of IgG was run on each type of gel to ensure that disulfide bonds remained intact under non-reducing conditions.

Mass Spectrometry — Reduced and oxidized apo H-NOX were generated as above, except that tris(2-carboxyethyl)phosphine (TCEP) was used as reductant in place of DTT for one sample. Samples were desalted into deionized water using Zeba™ spin desalting columns (Pierce). Acetonitrile and formic acid were added to 50% and 0.1%, respectively, and the samples were analyzed by direct infusion electrospray ionization Fourier transform ion cyclotron resonance mass spectrometry (ESI FT-ICR MS) in the positive ionization mode. FT-ICR MS was performed with a hybrid linear ion trap FT-ICR mass spectrometer (LTQ FT, Thermo Fisher, San Jose, CA) equipped with a 7 Tesla superconducting magnet. Direct infusion of the samples was performed with an Advion Triversa Nanomate (Advion, Ithaca, NY). Positive–ion ESI mass spectra were recorded for

quadrupole-selected charge state clusters at mass resolving power, $m/\Delta m_{50\%}$ = 400,000 at m/z 400. Two hundred time domain transients were co-added prior to fast Fourier transformation and frequency to m/z conversion.

Pull-down Assay — Four small columns were prepared each containing 100 µL of Ni-NTA resin equilibrated with storage buffer plus 10 mM imidazole. Four samples were prepared containing 100 µL of 50 µM untagged apo H-NOX in the reduced or oxidized states, either alone or in the presence of 50 µM HnoK. These were incubated on ice prior to application to the Ni-NTA resin. The column was washed with 10 cv of storage buffer plus 10 mM imidazole and eluted with 6 cv of storage buffer plus 250 mM imidazole. Elution fractions were concentrated and total protein concentrations determined by Bradford assay (38). This was used to normalize total protein amounts loaded on the gel for HnoK-containing samples. The elution fractions from control samples lacking HnoK were concentrated to the same final volume as those containing HnoK for loading onto the gel.

Acknowledgments ─ We acknowledge the Office of the Vice President for Research and the Center for Animal Health and Food Safety at New Mexico State University as well as the National Science Foundation (IIA-1301346) for funding this study. Our thanks also go to Natalie van Rompaey for technical assistance and lab management and to the DNA sequencing facility at New Mexico State University for mutagenesis.

Conflict of Interest ─ The authors declare that they have no conflicts of interest with the contents of this article.

Author Contributions ─ RM and ETY performed and analyzed experiments. NS and TS performed mass spectrometry measurements. ETY conceived and coordinated the study and wrote the paper.

REFERENCES

1. Tennyson, A. G., and Lippard, S. J. (2011) Generation, translocation, and action of nitric oxide in living systems. *Chem. Biol.* **18**, 1211-1220
2. Furchgott, R. F. (1999) Endothelium-derived relaxing factor: discovery, early studies, and identification as nitric oxide. *Biosci. Rep.* **19**, 235-251
3. Lucas, K. A., Pitari, G. M., Kazerounian, S., Ruiz-Stewart, I., Park, J., Schulz, S., Chepenik, K. P., and Waldman, S. A. (2000) Guanylyl cyclases and signaling by cyclic GMP. *Pharmacol. Rev.* **52**, 375-414
4. Derbyshire, E. R., and Marletta, M. A. (2012) Structure and regulation of soluble guanylate cyclase. *Annu. Rev. Biochem.* **81**, 533-559
5. Iyer, L. M., Anantharaman, V., and Aravind, L. (2003) Ancient conserved domains shared by animal soluble guanylyl cyclases and bacterial signaling proteins. *BMC genomics* **4**, 5
6. Carlson, H. K., Vance, R. E., and Marletta, M. A. (2010) H-NOX regulation of c-di-GMP metabolism and biofilm formation in Legionella pneumophila. *Mol. Microbiol.*
7. Henares, B. M., Higgins, K. E., and Boon, E. M. (2012) Discovery of a nitric oxide responsive quorum sensing circuit in Vibrio harveyi. *ACS Chem. Biol.* **7**, 1331-1336
8. Liu, N., Xu, Y., Hossain, S., Huang, N., Coursolle, D., Gralnick, J. A., and Boon, E. M. (2012) Nitric oxide regulation of cyclic di-GMP synthesis and hydrolysis in Shewanella woodyi. *Biochemistry* **51**, 2087-2099
9. Plate, L., and Marletta, M. A. (2012) Nitric oxide modulates bacterial biofilm formation through a multicomponent cyclic-di-GMP signaling network. *Mol. Cell* **46**, 449-460
10. Plate, L., and Marletta, M. A. (2013) Nitric oxide-sensing H-NOX proteins govern bacterial communal behavior. *Trends Biochem. Sci.* **38**, 566-575

11. Price, M. S., Chao, L. Y., and Marletta, M. A. (2007) Shewanella oneidensis MR-1 H-NOX regulation of a histidine kinase by nitric oxide. *Biochemistry* **46**, 13677-13683
12. Herzik, M. A., Jr., Jonnalagadda, R., Kuriyan, J., and Marletta, M. A. (2014) Structural insights into the role of iron-histidine bond cleavage in nitric oxide-induced activation of H-NOX gas sensor proteins. *Proc. Natl. Acad. USA* **111**, E4156-4164
13. Wu, G., Liu, W., Berka, V., and Tsai, A. L. (2013) The Selectivity of Vibrio cholerae H-NOX for Gaseous Ligands Follows the "Sliding Scale Rule" Hypothesis. Ligand Interactions with both Ferrous and Ferric Vc H-NOX. *Biochemistry* **52**, 9432-9446
14. Tsai, A. L., Berka, V., Martin, F., Ma, X., van den Akker, F., Fabian, M., and Olson, J. S. (2010) Is Nostoc H-NOX a NO sensor or redox switch? *Biochemistry* **49**, 6587-6599
15. Cremers, C. M., and Jakob, U. (2013) Oxidant sensing by reversible disulfide bond formation. *J. Biol. Chem.* **288**, 26489-26496
16. Hightower, K. E., and Fierke, C. A. (1999) Zinc-catalyzed sulfur alkyation:insights from protein farnesyltransferase. *Curr. Opin. Chem. Biol.* **3**, 176-181
17. Rozema, D. B., and Poulter, C. D. (1999) Yeast protein farnesyltransferase. pKas of peptide substrates bound as zinc thiolates. *Biochemistry* **38**, 13138-13146
18. Giles, N. M., Watts, A. B., Giles, G. I., Fry, F. H., Littlechild, J. A., and Jacob, C. (2003) Metal and redox modulation of cysteine protein function. *Chem. Biol.* **10**, 677-693
19. Graumann, J., Lilie, H., Tang, X., Tucker, K. A., Hoffmann, J. H., Vijayalakshmi, J., Saper, M., Bardwell, J. C., and Jakob, U. (2001) Activation of the redox-regulated molecular chaperone Hsp33--a two-step mechanism. *Structure* **9**, 377-387
20. Ilbert, M., Horst, J., Ahrens, S., Winter, J., Graf, P. C., Lilie, H., and Jakob, U. (2007) The redox-switch domain of Hsp33 functions as dual stress sensor. *Nat. Struct. Mol. Biol.* **14**, 556-563
21. Winter, J., Ilbert, M., Graf, P. C., Ozcelik, D., and Jakob, U. (2008) Bleach activates a redox-regulated chaperone by oxidative protein unfolding. *Cell* **135**, 691-701
22. Pother, D. C., Liebeke, M., Hochgrafe, F., Antelmann, H., Becher, D., Lalk, M., Lindequist, U., Borovok, I., Cohen, G., Aharonowitz, Y., and Hecker, M. (2009) Diamide triggers mainly S Thiolations in the cytoplasmic proteomes of Bacillus subtilis and Staphylococcus aureus. *J. Bacteriol.* **191**, 7520-7530
23. Tortorella, D., Story, C. M., Huppa, J. B., Wiertz, E. J., Jones, T. R., Bacik, I., Bennink, J. R., Yewdell, J. W., and Ploegh, H. L. (1998) Dislocation of type I membrane proteins from the ER to the cytosol is sensitive to changes in redox potential. *J. Cell. Biol.* **142**, 365-376
24. Barbirz, S., Jakob, U., and Glocker, M. O. (2000) Mass spectrometry unravels disulfide bond formation as the mechanism that activates a molecular chaperone. *J. Biol. Chem.* **275**, 18759-18766
25. Jakob, U., Eser, M., and Bardwell, J. C. (2000) Redox switch of hsp33 has a novel zinc-binding motif. *J. Biol. Chem.* **275**, 38302-38310
26. Jakob, U., Muse, W., Eser, M., and Bardwell, J. C. (1999) Chaperone activity with a redox switch. *Cell* **96**, 341-352
27. Pattison, D. I., and Davies, M. J. (2001) Absolute rate constants for the reaction of hypochlorous acid with protein side chains and peptide bonds. *Chem. Res. Toxicol.* **14**, 1453-1464
28. Lesser, M. P. (2006) Oxidative stress in marine environments: biochemistry and physiological ecology. *Annu. Rev. Physiol.* **68**, 253-278

29. Allaoui, A., Botteaux, A., Dumont, J. E., Hoste, C., and De Deken, X. (2009) Dual oxidases and hydrogen peroxide in a complex dialogue between host mucosae and bacteria. *Trends Mol. Med.* **15**, 571-579
30. El Hassani, R. A., Benfares, N., Caillou, B., Talbot, M., Sabourin, J. C., Belotte, V., Morand, S., Gnidehou, S., Agnandji, D., Ohayon, R., Kaniewski, J., Noel-Hudson, M. S., Bidart, J. M., Schlumberger, M., Virion, A., and Dupuy, C. (2005) Dual oxidase2 is expressed all along the digestive tract. *Am. J. Physiol. Gastrointest. Liver Physiol.* **288**, G933-942
31. Yildiz, F. H., and Schoolnik, G. K. (1999) Vibrio cholerae O1 El Tor: identification of a gene cluster required for the rugose colony type, exopolysaccharide production, chlorine resistance, and biofilm formation. *Proc. Natl. Acad. USA* **96**, 4028-4033
32. Edelhoch, H. (1967) Spectroscopic determination of tryptophan and tyrosine in proteins. *Biochemistry* **6**, 1948-1954
33. Furhrhop J.H., S., K.M. (1975) *Laboratory Methods in Porphyrin and Metalloporphyrin Research.*, Elsevier Scientific Publishing Co., Amsterdam, New York
34. Hildebraunt, A. G., and Roots, I. (1975) Reduced nicotinamide adenine dinucleotide phosphate (NADPH)-dependent formation and breakdown of hydrogen peroxide during mixed function oxidation reactions in liver microsomes. *Arch. Biochem. Biophys.* **171**, 385-397
35. Morris, J. C. (1966) The Acid Ionization Constant of HOCl from 5 to 35°. *J. Phys. Chem.* **70**, 3798-3805
36. Riddles, P. W., Blakeley, R. L., and Zerner, B. (1979) Ellman's reagent: 5,5'-dithiobis(2-nitrobenzoic acid)--a reexamination. *Anal. Biochem.* **94**, 75-81
37. Riddles, P. W., Blakeley, R. L., and Zerner, B. (1983) Reassessment of Ellman's reagent. *Methods Enzymol.* **91**, 49-60
38. Bradford, M. M. (1976) A rapid and sensitive method for the quantitation of microgram quantities of protein utilizing the principle of protein-dye binding. *Anal. Biochem.* **72**, 248-254
39. Arnold, K., Bordoli, L., Kopp, J., and Schwede, T. (2006) The SWISS-MODEL workspace: a web-based environment for protein structure homology modelling. *Bioinformatics* **22**, 195-201

FOOTNOTES

[1]To whom correspondence should be addressed: Erik T. Yukl, Department of Chemistry and Biochemistry, 1175 N. Horseshoe Dr, Las Cruces, New Mexico 88003. Tel. 575 646 3176; Fax. 575 646 2649; E-mail: etyukl@nmsu.edu

[2]The abbreviations used are: H-NOX, heme nitric oxide / oxygen; HisKa, histidine kinase; NO nitric oxide; DEA-NONOate, diethylamine NONOate; sGC, soluble guanylate cyclase; cGMP, cyclic guanosine monophosphate; c-di-GMP, cyclic di-guanosine monophosphate; *Vc, Vibrio cholerae; So, Shewanella oneidensis*; DTT, dithiothreitol; ICP-OES, inductively coupled plasma-optical emission spectroscopy; CD, circular dichroism; DTNB, 5,5'-dithio-bis-[2-nitrobenzoic acid]; TCEP, Tris(2-carboxyethyl)phosphine.

FIGURE LEGENDS

Figure 1. Purification and characterization of H-NOX and HnoK. (A) SDS-PAGE of MW ladder (lane 1) purified HnoK (lane 2), holo H-NOX (lane 3) and apo H-NOX (lane 4). (B) Absorption spectra of holo H-NOX in the Fe(III) (solid line) and Fe(II)-NO (dotted line) forms at 10 μM and apo H-NOX (dashed line) at 20 μM. (C) Circular dichorism spectra of WT and C177A holo and apo H-NOX. (D) Autophosphorylation of HnoK over time in the presence and absence of 1 mM DTT.

Figure 2. Homology model of the zinc site of *Vc* H-NOX using *So* H-NOX (PDB code 4U99) as a model. Residues that are identical in the *So* H-NOX structure are indicated with an asterisk. The model was made using SWISS-MODEL (39).

Figure 3. Quantitation of iron (blue), zinc (red) and DTNB-reactive thiol under native (green) and denaturing (purple) conditions for various preparations of holo and apo WT (A) and C177A (B) H-NOX. Fe and Zn values for the Fe(II)-NO forms were assumed to be identical to Fe(III) and were not measured. Experiments were performed in duplicate on independent protein preparations and error bars represent the standard error between measurements.

Figure 4. Inhibition of HnoK autophosphorylation by holo and apo H-NOX. Autophosphorylation of 10 μM HnoK after 1 hr was monitored in the presence of increasing concentrations WT (A) and C177A (C) holo H-NOX in the Fe(III) (blue) and Fe(II)-NO (red) forms or WT apo as-isolated (green). Inhibition by WT(B) and C177A (D) apo H-NOX reduced with DTT (blue) and oxidized with H_2O_2 (red), diamide (green) and HOCl (purple). Experiments were performed in duplicate and error bars represent the standard error between measured band intensities from duplicate experiments.

Figure 5. WT Fe(III) H-NOX (dotted line) reacts with 1 mM DTT under anaerobic conditions to yield Fe(II) H-NOX (dashed line). Exposure to air causes a shift and decrease in heme absorbance (solid lines, scans taken every 30 minutes). Arrows indicate the direction of absorbance changes with time.

Figure 6. (A) Absorption spectra of C177A holo H-NOX in the Fe(III) (solid line) and Fe(II)-NO (dotted line) forms at 10 μM and apo H-NOX (dashed line) at 20 μM. (B) C177A Fe(III) H-NOX (dotted line) reacts with 1 mM DTT under anaerobic conditions to yield Fe(II) H-NOX (dashed line). Exposure to air causes a shift and decrease in heme absorbance (solid lines, scans taken every 30 minutes). Arrows indicate the direction of absorbance changes with time.

Figure 7. Whole protein mass spectra showing the +22 charge state of WT (A) and C177A (B) apo H-NOX reduced with DTT (blue) and oxidized with H_2O_2 (red), diamide (green) and HOCl (purple). Gray x marks indicate the expected isotope profile for H-NOX protein sequences bearing the monoisotopic mass indicated in the figure. Each measurement represents a single sample.

Figure 8. Whole protein mass spectra showing an expanded view of the +22 charge state of WT (A) and C177A (B) apo H-NOX reduced with DTT (blue) and oxidized with diamide (green). WT apo H-NOX reduced with TCEP and reoxidized with diamide (C).

Figure 9. Non-reducing SDS-PAGE of WT (lanes 1-6) and C177A (lanes 7-12) H-NOX in the following forms: holo as-isolated (1,7), apo as-isolated (2,8), apo DTT-reduced (3,9), apo oxidized with H_2O_2 (4,10), diamide (5,11) and HOCl (6,12). Arrows indicate the expected positions of monomeric and dimeric H-NOX species as labeled.

Figure 10. Pulldown assay. MW ladder (lanes 1 and 8), 4 μg of purified untagged apo H-NOX (lane 2) and His-tagged HnoK (lane 3). Concentrated elution fractions for untagged apo H-NOX alone in the

reduced (lane 4) and HOCl-oxidized states (lane 5). 8 μg of elution fractions from HnoK + reduced H-NOX (lane 6) and HnoK + HOCl-oxidized H-NOX (lane 7). Asterisks indicate the position of a ~ 27 kDa contaminant found in all HnoK-containing lanes.

Figure 11. Proposed mechanism for heme-independent redox sensing by apo *Vc* H-NOX.

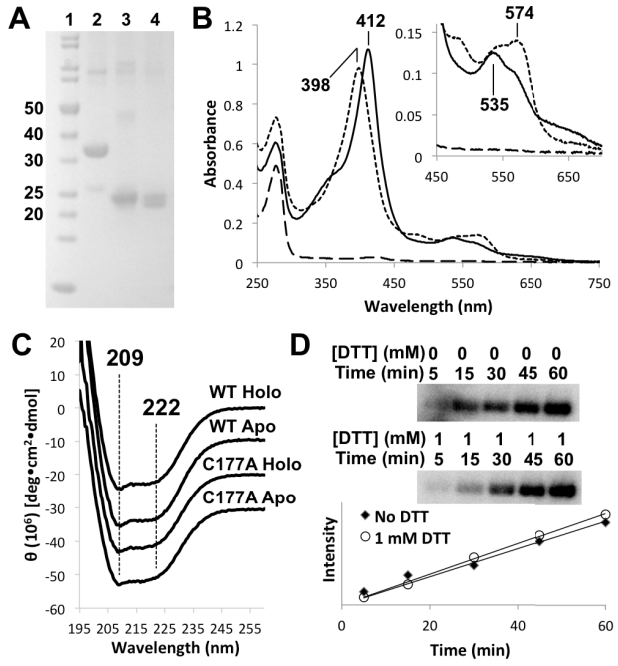

Figure 1

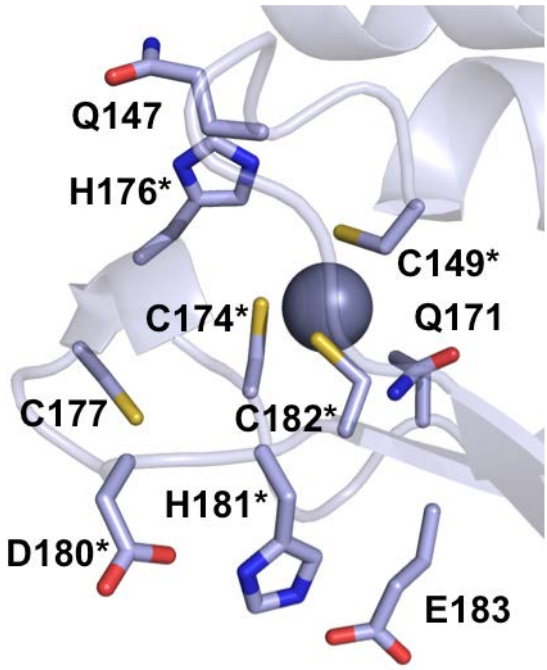

Figure 2

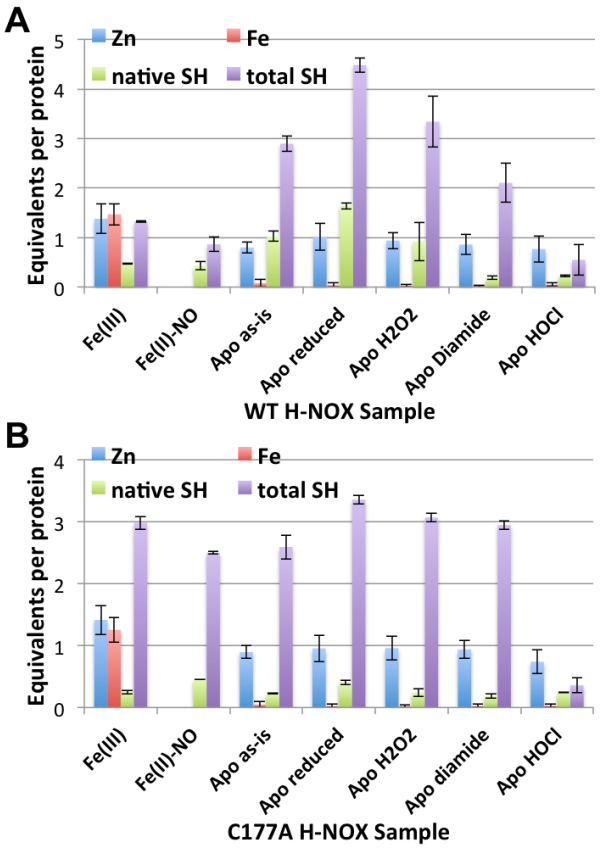

Figure 3

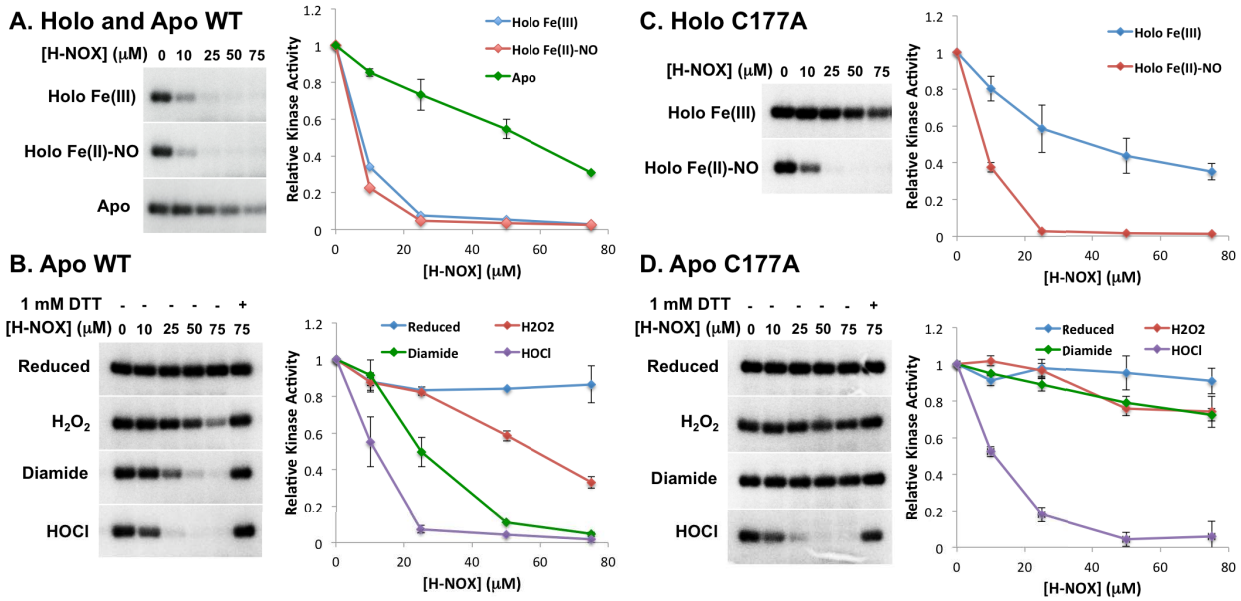

Figure 4

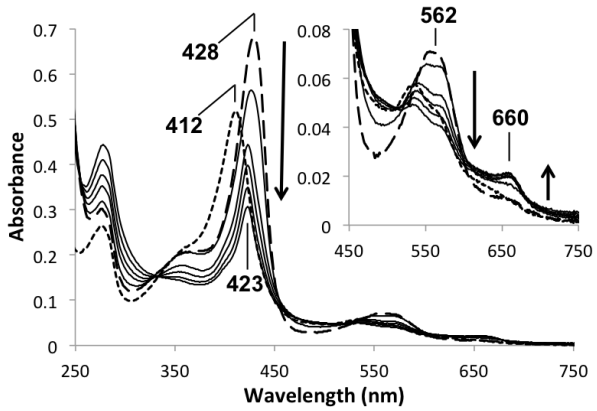

Figure 5

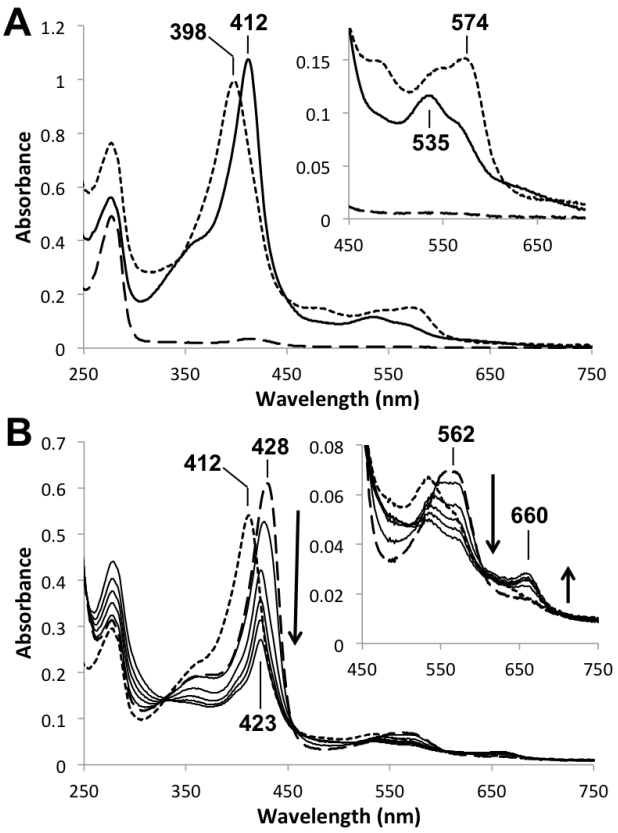

Figure 6

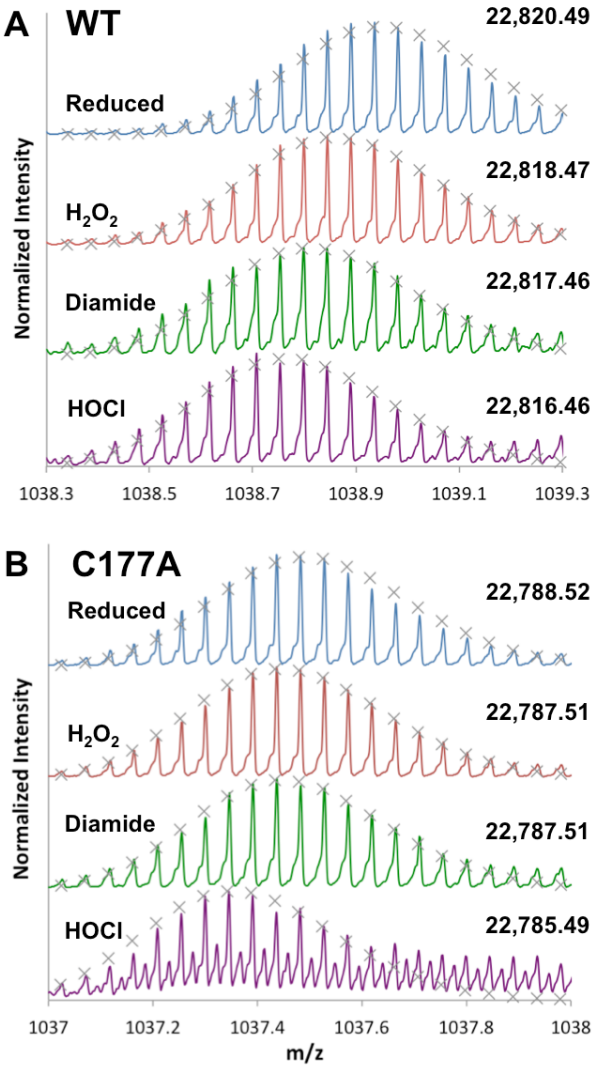

Figure 7

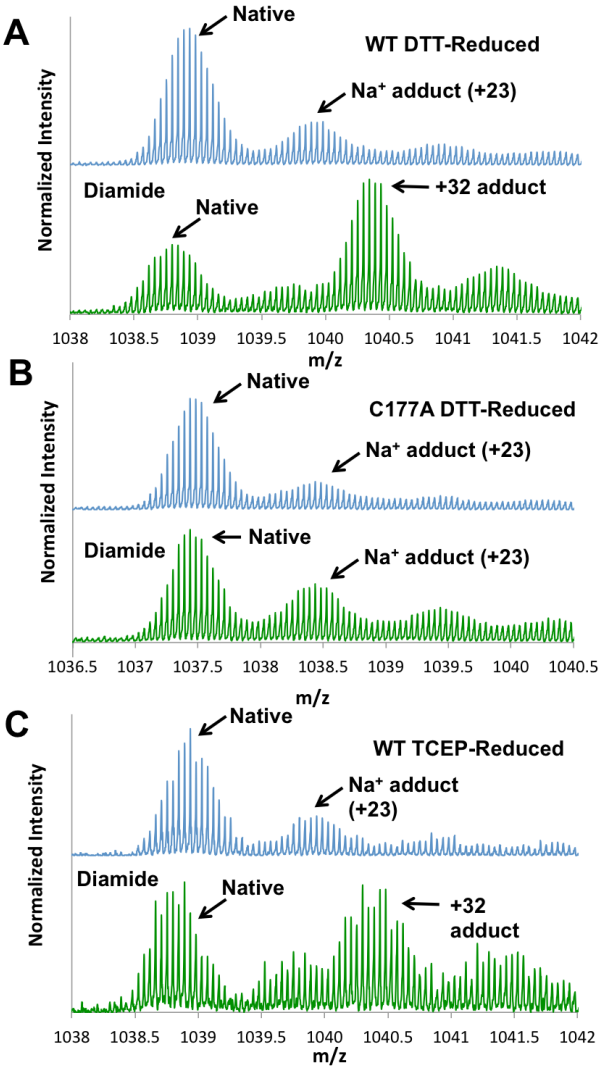

Figure 8

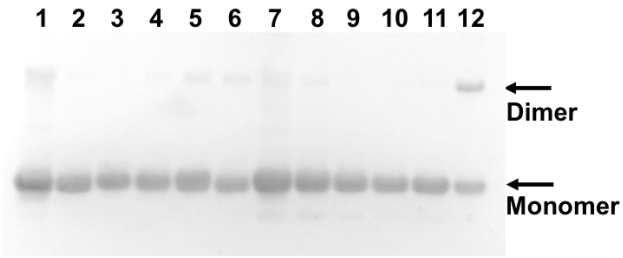

Figure 9

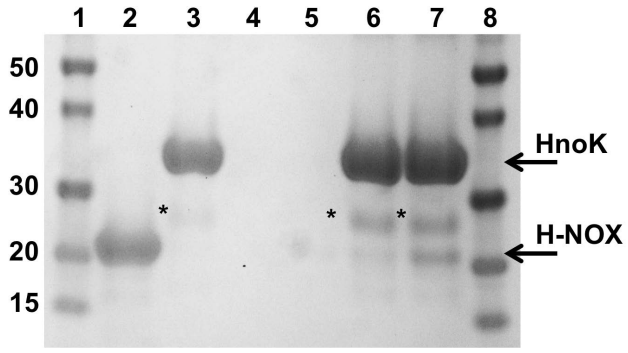

Figure 10

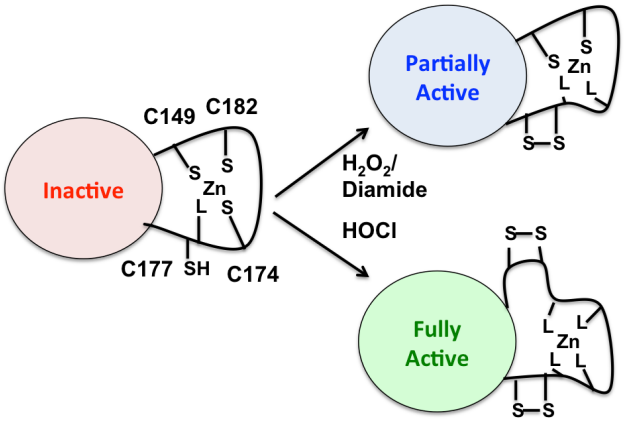

Figure 11

Heme-Independent Redox Sensing by the Heme-Nitric Oxide/Oxygen Binding Protein (H-NOX) from Vibrio cholerae

Roma Mukhopadhyay, Nilusha Sudasinghe, Tanner Schaub and Erik T. Yukl

J. Biol. Chem. published online June 29, 2016
